Paleoceanography and Paleoclimatology

RESEARCH ARTICLE
10.1029/2018PA003497

Millennial-Scale Climate Variability and Dinoflagellate-Cyst-Based Seasonality Changes Over the Last ~150 kyrs at "Shackleton Site" U1385

Mariska Datema[1], Francesca Sangiorgi[1], Anne de Vernal[2], Gert-Jan Reichart[3,4], Lucas J. Lourens[3], and Appy Sluijs[1]

[1]Marine Palynology and Paleoceanography, Laboratory of Palaeobotany and Palynology, Department of Earth Sciences, Faculty of Geosciences, Utrecht University, Utrecht, The Netherlands, [2]Centre de recherche en géochimie et géodynamique (Geotop), Université du Québec à Montréal, Montréal, Quebec, Canada, [3]Department of Earth Sciences, Faculty of Geosciences, Utrecht University, Utrecht, The Netherlands, [4]Department of Ocean Systems, NIOZ Royal Netherlands Institute for Sea Research, Texel, The Netherlands

Key Points:
- New high-resolution dinocyst-based summer and winter SST record from IODP "Shackleton" Site U1385 for the last 150 kyrs is presented
- Dinocyst-based SST confirms the D-O cycles and HEs at Site U1385
- Increased seasonal contrast of SST (up to 12 degree C) during cold periods of the glacial cycle related to strong winter cooling is shown

Supporting Information:
- Supporting Information S1

Correspondence to:
M. Datema,
m.c.datema@uu.nl

Citation:
Datema, M., Sangiorgi, F., de Vernal, A., Reichart, G.-J., Lourens, L. J., & Sluijs, A. (2019). Millennial-scale climate variability and dinoflagellate-cyst-based seasonality changes over the last ~150 kyrs at "Shackleton Site" U1385. *Paleoceanography and Paleoclimatology*, *34*, 1139–1156. https://doi.org/10.1029/2018PA003497

Received 19 OCT 2018
Accepted 15 MAY 2019
Accepted article online 29 MAY 2019
Published online 16 JUL 2019

Abstract During the last glacial period, climate conditions in the North Atlantic region were determined by the alternation of relatively warm interstadials and relatively cool stadials, with superimposed rapid warming (Dansgaard-Oeschger) and cooling (Heinrich) events. So far little is known about the impact of these rapid climate shifts on the seasonal variations in sea surface temperature (SST) within the North Atlantic region. Here, we present a high-resolution seasonal SST record for the past 152 kyrs derived from Integrated Ocean Drilling Program "Shackleton" Site U1385, offshore Portugal. Assemblage counts of dinoflagellates cysts (dinocysts) in combination with a modern analog technique (MAT), and regression analyses were used for the reconstructions. We compare our records with previously published SST records from the same location obtained from the application of MAT on planktonic foraminifera. Our dinocyst-based reconstructions confirm the impression of the Greenland stadials and interstadials offshore the Portuguese margin and indicate increased seasonal contrast of temperature during the cold periods of the glacial cycle (average 9.0 °C, maximum 12.2 °C) with respect to present day (5.1 °C), due to strong winter cooling by up to 8.3 °C. Our seasonal temperature reconstructions are in line with previously published data, which showed increased seasonality due to strong winter cooling during the Younger Dryas and the Last Glacial Maximum over the European continent and North Atlantic region. In addition, we show that over longer time scales, increased seasonal contrasts of temperature remained characteristic of the colder phases of the glacial cycle.

1. Introduction

Reliable reconstructions of past climates are needed for better constraining future climate change. Past reconstructions are mostly expressed in terms of annual means, as proxies for temperature, productivity, salinity, and other parameters are often calibrated against their mean annual values (e.g., Intergovernmental Panel on Climate Change, IPCC, 2013; Carré & Cheddadi, 2017). However, seasonal-scale processes may impact climate variability well beyond the annual cycle and contribute to large-scale climate shifts (e.g., orbital forcing of climate, inception of glacials; Huybers & Curry, 2006; Carré & Cheddadi, 2017). Present-day climate is changing due to anthropogenic influences and this includes pronounced changes in seasonality (IPCC, 2013; Santer et al., 2018). This is important because seasonal extremes control habitability of regions as well as stability of ice sheets. Hence, changes in seasonality in the geological past merit investigation.

A large effort has already been made to unravel past seasonality, especially on the relatively recent time intervals such as the Holocene, Younger Dryas (YD), and the Last Glacial Maximum (LGM) (e.g., Birks & Koç, 2002; de Vernal et al., 2005, 2006; Koç, Karpuz & Jansen, 1992; Koc et al., 1993; Kucera et al., 2005; Meland et al., 2005; Penaud et al., 2010; Penaud, Eynaud, Voelker, et al., 2011; Pflaumann et al., 2003; Sarnthein et al., 2003; van Nieuwenhove et al., 2016; Vogelsang et al., 2001). Some summer-winter sea surface temperature (SST) reconstructions based on planktic foraminifers go further back in time but do not show any substantial seasonality changes (e.g., Cayre et al., 1999; Kandiano & Bauch, 2003; Voelker & de Abreu, 2011; Waelbroeck et al., 1998). This seems unrealistic and may be an artifact of

the strong correlation of winter and summer temperatures in the modern foraminifer database used for reconstructing SSTs with modern analog technique (MAT) or transfer functions (e.g., Guiot & de Vernal, 2007; Kucera et al., 2005). Indeed, comparing and combining different proxy records show that the seasonal component of past climate change can be large (e.g., Denton et al., 2005). Several studies on glacial climate states suggested increased seasonality as result of stronger cooling during winters that may have been fostered by enhanced stratification and lower thermal inertia (e.g., Broecker, 2006; Combourieu-Nebout et al., 2002; Denton et al., 2005; de Vernal et al., 2005; Mix et al., 1986; Pérez-Folgado et al., 2002; Penaud, Eynaud, Sanchez Goñi, et al., 2011; Wary et al., 2015). However, to the best of our knowledge, a reconstruction of summer versus winter temperature from the North Atlantic over the full last glacial cycle based on a single proxy that shows substantial changes in seasonality is still lacking.

Seasonal changes affect plants and animals, resulting in phenological shifts that can be reconstructed to study climate change and determine seasonality (Donnelly & Yu, 2017). However, the number of records and methods that are suitable to reliably disentangle past seasonal climate components is limited. For example, rapidly accumulating paleoclimate archives are used from which seasonal resolution can be obtained. This is the case for corals (Beck et al., 1992; Corège et al., 2004; Felis et al., 2004; Lazareth et al., 2013; Sun et al., 2005), some speleothems (Ridley et al., 2015), and ice cores (Morgan & van Ommen, 1997). Such records directly resolve the various seasons throughout the year, but can still be hampered by hiatuses, a lack of growth/accretion during a specific season, and dampening of the seasonal component of the signal in case the records are not analyzed with sufficient resolution. Hence, true seasonality is difficult to obtain from a single proxy record. An indirect approach, based on fossil assemblages, does not necessarily suffer from such biases and can reconstruct past seasonal changes without generating annual resolution data sets.

MAT applied to assemblages from sediment cores enable to reconstruct seasonal temperatures providing that summer and winter temperature do not correlate in the reference database and assuming assumption that seasonality is a determining factor of faunal and floral assemblages. This is particularly true at the middle to high latitudes, where the seasonal cycle regulates local and regional conditions and, hence, the distribution of taxa. Using modern observations of taxa distributions, the MAT can be used to reconstruct past climate variables, including not only annual means but also seasonal values (e.g., de Vernal et al., 2000, 2001, 2005; de Vernal, Hillaire-Marcel, et al., 2013; de Vernal, Rochon, et al., 2013). Such approaches can apply to different types of fossil assemblages, as long as the organisms considered show sufficiently large phenological shifts. Summer and winterSSTs were reconstructed by applying the MAT on foraminifer assemblages for the entire North Atlantic for the LGM (Meland et al., 2005; Pflaumann et al., 2003; Sarnthein et al., 2003). However, the same method applied to foraminifera for the reconstruction of the past 150 thousand years (kyrs) hardly shows substantial changes in seasonality (e.g., Cayre et al., 1999; Voelker & de Abreu, 2011). This is not surprising in view of the interdependency of winter and summer temperature and uniform seasonal gradients in the reference data set. For the West Iberian Margin (WIM), Datema et al. (2017) used dinoflagellate cysts (dinocysts) to reconstruct summer and winter SSTs at the scale of the last 22 kyrs, indicating stronger cooling in winter than in summer during the LGM. While results are promising, this approach has not yet been widely applied, spatially and/or temporally (Carré & Cheddadi, 2017).

In this study we constructed a millennial-scale seasonality record for the WIM using dinocyst summer and winter MAT-based SSTs, extending the Datema et al. (2017) record to cover the full last glacial cycle. We use sediments deposited over the last 152 kyr at the Integrated Ocean Drilling Program (IODP) Site U1385 (Hodell, Crowhurst, et al., 2013) along the WIM. The average temporal resolution of palynological analyses is 600 years. Dinocyst assemblages were analyzed to reconstruct summer and winter SSTs using a MAT approach and the Modern $n = 1492$ database of de Vernal, Hillaire-Marcel, et al. (2013) and de Vernal, Rochon, et al. (2013). At the same time, we generated SST estimates based on a qualitative approach (warm/cold SSTdino index from dinocyst abundances). This continuous record allows us to investigate changes in seasonality on a millennial-scale interval across the entire last glacial cycle. We compare the seasonal contrast between the cold Greenland/Heinrich stadials offshore Portugal over the entire glacial cycle with present-day conditions and the warmer interstadials. The overall aim of this work is to reconstruct changes in seasonality at the midlatitudes and its potential role in climate change on a millennial time scale through the last glacial-interglacial cycle.

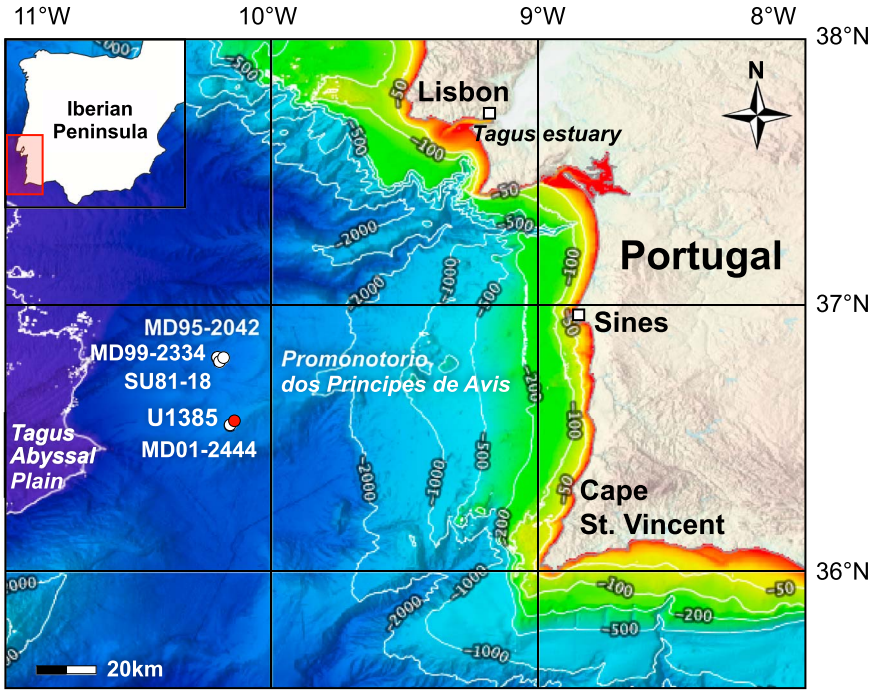

Figure 1. West Iberian Margin showing the location of Shackleton Site U1385 and nearby sites. The map shows the Iberian Peninsula, the location of Shackleton Site U1385 (red circle, this study), other sites discussed in the text (white circles), depth (blue color for deeper zones), isobaths (50, 100, 200, 500, 1,000, and 2,000 m) and some of the main topographic features. The bathymetric metadata and Digital Terrain Model data products were derived from the EMODnet Bathymetry portal (http://www.emodnet-bathymetry.eu). Figure adapted from Datema et al. (2017).

2. Oceanographic Setting

Atmospheric and oceanographic circulation in the North Atlantic Ocean are largely determined by the North Atlantic Oscillation. The Azores high and Icelandic low atmospheric pressure cells, linked to the North Atlantic Subtropical and Polar Gyres, respectively, vary in strength and control the direction of winds across the North Atlantic (Arístegui et al., 2005). The different North Atlantic Oscillation phases, positive or negative, change the intensity and location of the North Atlantic jet stream and storm track resulting in variations in the zonal and meridional heat and moisture transport. This affects climatic conditions over the ocean and the adjacent continents. At present day average seasonality (summer-winter SST) in the North Atlantic (from ~6–30°W) ranges from 0 °C at the equatorial and polar latitudes to 6 °C at 40°N. The WIM (~37–44°N) is situated in the northern part of the North Atlantic Subtropical Gyre, where the mean seasonal gradient of SST is ~5.1 °C.

In the western North Atlantic, the Gulf Stream branches off into the North Atlantic Current toward the northeast and the Azores Current toward the southeast. The zone between the North Atlantic Current and the Azores Current is marked by weak circulation supplying the large-scale Portugal Current System that represents the surface currents along the WIM (Pérez et al., 2001; Figure 2 in Datema et al., 2017). The WIM has a narrow continental shelf with a steep upper slope that is intersected by promontories and indented by canyons (Figure 1). Direction of flow over the narrow continental shelf changes seasonally (Peliz et al., 2005; Teles-Machado, Peliz, McWilliams, Couvelard, et al., 2015).

In summer (July–September) the Azores High is strong and the resulting intense northerly Portuguese Trade Winds induce upwelling as a result of offshore Ekman transport (Arístegui et al., 2005; Arístegui et al., 2009; Relvas et al., 2007; Teles-Machado, Peliz, McWilliams, Cardoso, et al., 2015). Filaments of upwelled cool and nutrient-rich water sometimes extend more than 200 km offshore at promontories and canyons and fuel primary production (Relvas et al., 2007; Sousa & Bricaud, 1992). The coastal jet current flows southward over the shelf. In winter (September–January), the Azores High is weak and the resulting westerly/southerly winds intensify the northward Iberian Poleward Current that ceases upwelling (Arístegui et al., 2009;

Peliz et al., 2005; Relvas et al., 2007; Teles-Machado, Peliz, McWilliams, Couvelard, et al., 2015, Teles-Machado, Peliz, McWilliams, Cardoso, et al., 2015).

Present-day summer sea surface temperatures (SST_{su}) at the WIM average 20.4 ± 0.2 °C and winter temperatures (SST_{wi}) are 15.3 ± 0.2 °C (World Ocean Database: Boyer et al., 2013). These are seasonal averages near Site U1385; however, sea surface parameters can vary locally and temporally due to variable extent of upwelling filaments and meandering sea surface fronts (Peliz et al., 2005). SSTs of upwelled waters close to the Portuguese coast and off Cape St. Vincent are around 15–18 °C and can influence SSTs at Site U1385 (Relvas et al., 2007; Sánchez et al., 2008; Sánchez & Relvas, 2003).

3. Material and Methods

3.1. Site U1385

IODP Expedition 339 "Shackleton" Site U1385 (37°34.285′N, 10°7.562′W) is located on the continental slope of the southern WIM ~115 km off the nearest coast (Figure 1). The sea floor at the drill site is at 2,578 m below sea level on the Promontório dos Príncipes de Avis, which is above the abyssal plain and outside the influence of turbidite sedimentation. The site lies within the zone characterized by seasonal coastal upwelling and beyond the reach of the Mediterranean Outflow Water (Hodell, Crowhurst, et al., 2013).

IODP Site U1385 records a continuous sediment sequence spanning the past ~1.45 Ma, without hiatuses in the interval studied here (last 152 kyrs; Hodell et al., 2015). The sediment consists of nannofossil muds and clays, with varying proportions of biogenic carbonate and terrigenous components (Expedition 339 Scientists, 2013). A total of 252 samples was taken every 10 cm in the uppermost 24.20-meters composite depth (mcd) of the splice derived from Holes A and B (Table S1 in the supporting information).

3.2. Age Model of Site U1385

The Greenland synthetic (GreenSyn) age model of Site U1385 (Hodell et al., 2015) is based on correlation of the log (Ca/Ti) records of Sites MD01-2444 and U1385, through 20 tie points for the last 152 kyrs. In the present study, Greenland Stadials (GS) were identified in the log (Ca/Ti) record of Site U1385 taking into account the existing tie points between the log (Ca/Ti) records of Sites U1385 and MD01-2444 of Hodell et al. (2015) and between the $\delta^{18}O$ records of Site MD01-2444 and Greenland of Hodell, Lourens, et al. (2013). Subsequently, the alignment of Site U1385 to MD01-2444 (and hence also to the synthetic Greenland $\delta^{18}O$ temperature record of Barker et al., 2011) was improved by correlating GS with higher detail and adding 39 tie points between the log (Ca/Ti) records of Sites U1385 and MD01-2444 using our updated age model for site MD01-2444 (supporting information S1) and 17 original tie points of the Hodell et al. (2015) age model as basis for U1385 (Figure S1 and Table S2).

Ages for the 252 sampled intervals (Holes A and B splice) of Site U1385 were calculated using linear interpolation between the 56 tie points (Table S1). The resulting average sedimentation rate over the uppermost 24.20 mcd corresponding to the last 152 kyrs is 16 cm/kyr (Figure S2 and Table S2). The average time interval between the 252 samples of Site U1385 is 601 years.

3.3. Palynological Processing

The 252 sediment samples, ~12 grams each, were processed following the standard palynological procedure at the Laboratory of Palaeobotany and Palynology of Utrecht University, which includes spiking with a known amount of *Lycopodium* spores, 10% HCl and 38% cold HF treatment, and sieving over a 10-μm mesh sieve (see van Helmond et al., 2015 for details), without acetolysis or oxidation (see Zonneveld et al., 2008). These preparation techniques are the same as those used for the development of the standardized Northern Hemisphere database (e.g., Rochon et al., 1999; de Vernal et al., 2001, 2005; de Vernal, Hillaire-Marcel, et al., 2013; de Vernal, Rochon, et al., 2013; section 3.4.3).

Dinocysts were identified to the genus or species level, following the taxonomy of Rochon et al. (1999), Williams et al. (2017), and Zonneveld and Pospelova (2015). Microscopic slides were counted at 400X magnification to a minimum of 300 dinocysts and an average of ~490 dinocysts per sample, with the objective to achieve the highest counts possible for the taxa used for SST reconstructions (Table S3). All samples and slides are stored in the collection of the Laboratory of Palaeobotany and Palynology, Utrecht University, the Netherlands.

3.4. SST From Dinocyst Assemblage Counts

We reconstruct (seasonal) SST records for the past 152 kyrs from the assemblage counts of dinocysts of Site U1385 but based on three different methods: (1) definition of a qualitative warm/cold index using the assemblage counts of dinocysts to assess relative variations in SST (section 3.4.1); (2) quantification of this dinocyst index based on regression analyses (section 3.4.2); (3) application of the MAT to the whole assemblage counts, which provides quantitative SST independently from the index (section 3.4.3). Lastly, we combine approaches (2) and (3) to obtain one optimized qualitative SST record (section 3.4.4).

3.4.1. Qualitative Warm/Cold Index Based on Dinocysts

We assess relative variations in SST based on selected dinocyst taxa following Datema et al. (2017). The SST_{dino} index is defined as $SST_{dino} = n_w/(n_w+n_c)$, where n_w = number of "warm" taxa cysts and n_c = number of "cold" taxa cysts counted (for completeness, we reproduce Table 1 of Datema et al., 2017, indicating the composition of these groups in Table S3). SST dominantly drives the SST_{dino} index, although a small part of the variation might be related to SSS (Datema et al., 2017). The SST_{dino} index calculated on the dinocyst data set published in Eynaud et al. (2016), which covers large parts of our 152-kyr interval, shows very similar results (not shown) indicating the good reproducibility of our approach.

3.4.2. Quantification of the Dinocyst-Based SST Index Using Regression Analyses

Datema et al. (2017) calculated the SST_{dino} index on the modern Northern Hemisphere assemblages from the surface sediment data set of de Vernal, Hillaire-Marcel, et al. (2013) and de Vernal, Rochon, et al. (2013) and regressed it against summer and winter SST of the same samples. We use these regressions ($SST_{dino\_su} = (SST_{dino}+1.4443)/0.098$ and $SST_{dino\_wi} = (SST_{dino}+0.9287)/0.1155$) to quantify summer and winter SST from the qualitative SST_{dino} index (SST_{dino_su} and SST_{dino_wi} in degree Celsius) as calculated from the assemblage counts from Site U1385 for the past 152 kyrs. The possible ranges in SST that can be reconstructed using these quantifications are 14.74–24.94 °C for SST_{dino_su} and 8.04–16.70 °C for SST_{dino_wi} (see Datema et al., 2017). The estimated error is ± 2.35 °C for SST_{dino_su} and ±1.98 °C for SST_{dino_wi} (Figure S3a).

3.4.3. Quantitative SST Reconstruction Based on the MAT

Variations in sea surface water parameters are reconstructed using the MAT applied to whole dinocyst assemblages. The main assumption of the MAT is that similar assemblages likely occur under similar conditions (e.g., Guiot & de Vernal, 2007). The similarity between modern and fossil assemblages are analyzed by calculating the distance between the assemblages. Based on the smallest distance the five best analogs for the fossil assemblages are found in the modern data set. Subsequently, past surface water parameters are calculated based on a weighted average of the statistically significant modern analogs. The method, accuracy, and limitations of the MAT are described in detail in de Vernal et al. (2001, 2005), de Vernal, Hillaire-Marcel, et al. (2013) and de Vernal, Rochon, et al. (2013).

This study uses the updated standardized dinocyst data set from the Northern Hemisphere, which includes 1,492 surface samples from the North Atlantic, Arctic, and North Pacific Oceans, their adjacent seas and epicontinental environments (de Vernal, Hillaire-Marcel, et al., 2013; de Vernal, Rochon, et al., 2013). The geographic and hydrographic domains of the $n = 1492$ data set show sufficiently large ranges in SST for the reconstruction of glacial-interglacial values at the study site (SST ~ −2–31 °C, seasonality ~0–18 °C). Nomenclature and grouping of dinocyst taxa at Site U1385 are similar to the $n = 1492$ data set. The search for the five closest analogs is made based on 54 taxa. For more details on the use of the MAT and discussion of the quality of MAT reconstructions at Site U1385 (for the last 22 kyrs), see Datema et al. (2017). The numbers are slightly different for the 152 kyrs interval, but the same conclusions are valid.

The MAT is applied using scripts developed by Joël Guiot (CEREGE, France) for the software R (https://cran.r-project.org). The distance between the fossil and modern analog assemblages (d) and the threshold distance value (dT = 1.37) determine the quality of the reconstructions: analogs are good when $d = 0 - d$T/2, acceptable when $d = d$T/2 − dT and poor when $d > d$T (de Vernal et al., 2005; see also Datema et al., 2017). The majority (84%) of the found analogs are statistically significant within the given threshold ($d > d$T) and all reconstructions are based on average on four analogs, with a maximum of five analogs. Reconstructed variables are summer (July–September) and winter (January–March) SST (°C). We also reconstructed SST of the warmest and coldest months; however, the differences between these SSTs and summer and winter SST are not significant and within the errors of prediction. Hence, we will only use

summer and winter SST for our analyses. Based on the seasonal SST reconstructions, seasonality is calculated as the difference between summer and winter SST.

Importantly, the reference data set mainly includes sites from temperate to Arctic environments, while sites from the (warm) temperate and tropical environments are much less abundant. This limits the reconstruction of warm interglacial conditions: with the present data set dinocyst summer MAT has an upper limit of 18.8 °C and winter MAT has an upper limit of 15.3 °C (see also Datema et al., 2017). No lower limit is observed. This implies that data points for which summer and/or winter MAT are at or exceed these limits are unreliable. Therefore, seasonality was only calculated on data points below the summer and winter limits: seasonality was calculated for 91 of the 252 data points, including 57 data points for cold events and 34 data points for warm events. This also implies that not all Greenland (inter)stadials are included in the seasonality calculations, due to a lack of reliable data points in some of these intervals.

Correlation coefficients (R^2) between observations and reconstructions are 0.96 and 0.98 for SST in summer and winter (calculated using validation exercises on MAT applied to the $n = 1492$ data set, after log transformation of the data and search for the five best analogs, using the 54 taxa). The standard deviation of the difference between observations and reconstructions was used to calculate uncertainty estimates based on the errors of prediction. The errors of prediction are: ±1.63 °C and ±1.14 °C for SST in summer and winter (Figure S3b). Addition of the summer and winter errors of prediction (1.63 + 1.14 °C) gives the "maximum error of prediction" of MAT seasonality, which is ±2.77 °C. For all samples in this study seasonality calculated from the MAT is >2.77 °C and hence significant.

3.4.4. Composite Dinocyst SST Record

The quantified SST_{dino} index and MAT are strongly complementary at Site U1385; MAT can be used for reconstructions in colder periods, with a small error of prediction, and the quantified SST_{dino} index can be used to estimate SST for warmer periods beyond the limit of the MAT, though with much less precision (Datema et al., 2017). Hence, we combine SST reconstructions from the quantified SST_{dino} and dinocyst MAT SST into a composite dinocyst SST record (SST_C).

We use the quantified SST_{dino} when dinocyst MAT reconstructs SSTs near, at or above the MAT threshold (18.8 and 15.3 °C for summer and winter) and SST_{MAT} when dinocyst MAT reconstructs SSTs lower than the minimum SSTs that can be reconstructed with the quantified SST_{dino} (14.7 and 8.0 °C for summer and winter). For all SSTs between these two limits we used MAT SSTs, except for a few data points for which the quantified SST_{dino} is more in line with the stadial-interstadial variability as known from the Greenland ice core $\delta^{18}O$ record. The resulting composite dinocyst SST record (SST_C) consists for 73% of data points from the quantified SST_{dino} index and for 27% of data points from the MAT.

Reconstructing reliably SSTs at Site U1385 is not straightforward, because at times the site may have been under the influence of filaments of upwelled waters that have lower SSTs compared to the general offshore water temperatures (section 2). The reconstructed SSTs from both the quantified SST_{dino} index and MAT are based on the $n = 1492$ reference data set that possibly does not include sufficiently analogs to exclude a potential impact of upwelling (Figure C2 in Datema et al., 2017). Therefore, reconstructed sea surface parameters might be biased toward warmer (and more oligotrophic) conditions for periods when upwelling was more persistent than at the analog sites (see also Figure S3c).

The difference between summer and winter SSTs of the quantified SST_{dino} index depends on the regression equations (Datema et al., 2017) that are both calculated from the same SST_{dino} index. Therefore, seasonality calculated from the quantified SST_{dino} index, and hence also from SST_C, is artificial and constant through time. Hence, for the calculations of seasonality only SSTs reconstructed with MAT are used (section 3.4.3). However, for the discussion of potential seasonal biases of other proxies we do not consider the difference between summer and winter temperatures, but their absolute values, and we use SST_C instead of MAT-based SSTs.

4. Results

We found a total of 56 dinocyst taxa (Table S4). Dinocyst concentrations average ~6,200 and range between ~1,000 and 18,000 cysts per of gram dry sediment. The age model implies that accumulation rates average ~130 specimens·cm^{-2}·$year^{-1}$ and range between ~20 and 460 specimens·cm^{-2}·$year^{-1}$.

On average, over the studied interval, there is an equal amount of phototrophic (Gonyaulacoid) and heterotrophic (Protoperidinioid) dinocysts, although the relative abundances vary greatly through time, with an increasing abundance of heterotrophs toward the end of Marine Isotope Stage (MIS) 3 and MIS 2 and maximum abundances in the LGM (Figure S4). *Brigantedinium* spp. and *Lingulodinium machaerophorum* alternately dominate dinocyst assemblages throughout the record. Other abundant taxa are as follows: *Echinidinium* spp. and *Selenopemphix* spp. (heterotrophs) and *Spiniferites* spp. (mainly *S. ramosus*), *Impagidinium* spp. (mainly *I. aculeatum*), *Operculodinium* spp. (mainly *Operculodinium centrocarpum*), and *Nematosphaeropsis labyrinthus* (autotrophs). *Bitectatodinium tepikiense,* cysts of *Pentapharsodinium dalei*, *I. patulum* and *I. paradoxum* are the most abundant taxa included in the SST_{dino} index. The total abundance of warm and cold taxa used in the SST_{dino} index ranges from ~0–25% of the total assemblage, with an average of 6% (Table S5).

4.1. SSTs From Dinocysts

The SST_{dino} index shows clear variations in relative SST, both on the longer glacial-interglacial as the shorter millennial time scales (Figure 2a). The SST_{dino} index shows the highest relative SSTs in the interglacial MIS 5e and MIS 1 and lowest SSTs toward the end of MIS 3 and MIS 2, with distinct SST lows during almost all GS, such as the YD and Heinrich Stadials (HS).

The quantified SST_{dino} index is calculated from the SST_{dino} index and hence shows the same variability (Figure 2b). It reconstructs summer SSTs ranging from 14.7 °C (in the Last and Penultimate Glacial Maxima) to 24.4 °C (in MIS 1) and winter SSTs ranging from 8 °C (in MIS 6 and MIS 3-2) to 16.3 °C (in MIS 1), although this strongly depends on the regressions used (section 3.4.2).

SST from the MAT shows many intervals for which reconstructed SSTs are at the limit of the MAT (Figure 2c; Table S6). Only during MIS 5e the MAT reconstructs SSTs (~22 °C) higher than the limit that is seen in the rest of the record, but similar to the reconstructed SST from the quantified SST_{dino} index. Reconstructed summer SSTs are very similar for the quantified SST_{dino} index and the MAT, also for the intervals in which the MAT is at its limits. Only in MIS 1 the quantified SST_{dino} index reconstructs slightly higher SSTs. The MAT reconstructs larger drops in winter SSTs than summer SSTs for the cold intervals, mainly toward the end of MIS 3 and MIS 2, during (Heinrich) stadials and the LGM.

These results imply that the MAT approach likely underestimates summer and winter SST during warm phases and the quantified SST_{dino} likely underestimates cooling for cold phases. The composite dinocyst SST record (SST_C) combines reconstructions from the quantified SST_{dino} index and the MAT and therefore shows the best possible summer and winter SST reconstructions (Figure 2d). Indeed, our dinocyst records show almost all stadials and interstadials, notably including both distinct peaks and drops in SST in the warmer and colder intervals, respectively, corresponding well to the Log (Ca/Ti) record of the same site (Figure 2f), corroborating the robustness of our data. SST reconstructions range from a maximum of 24.4 °C for summer SST to a minimum of 3.4 °C for winter SST.

4.2. Seasonality in SST at Site U1385

Seasonality (Δ summer-winter) at Site U1385, as calculated from dinocyst MAT-based SST, ranges from 3.1 to 12.2 °C (Figure 2e). Seasonality is relatively high in cold intervals (GS and glacials, average of ~9.0 °C) compared to the warmer intervals (Greenland interstadials (GI) and interglacials, average of ~7.1 °C) and increases in MIS 3-2. Seasonality seems similar to present-day seasonality at the WIM (5.1 °C) in the interglacial MIS 5e and in MIS 1. However, it should be noted that the upper limit of summer and winter temperature in the MAT reference database are approached during the warmest phases of interglacials. This might imply that seasonality reduced even further during these phases than our minimum estimate of ~3.5 °C, which is defined by the maximum winter SST (15.3 °C) and maximum summer SST (18.8 °C) in the MAT model. Cold intervals show higher seasonality, with 9.0 °C in MIS 6, 7.7 °C in MIS 5d, 8.2 °C in the beginning of MIS 4, 8.3 °C in MIS 3, 8.5 °C in MIS 2, 9.0 °C in stadials (all averaged), and the highest average seasonality of 9.9 °C in HS.

Seasonality is increased in cold events due to the significantly larger decrease in winter SST (average -8.3 °C) than summer SST (average −4.4 °C) (Figures 2c and 3a). Only for the LGM the difference between summer and winter SST decrease is not significant (Figure 3a), while during HS this difference is especially large (Figure 3b). Considering the error of prediction, there are no significant differences in cooling between the different cold events. Only the decrease in SSTs of some of the earlier HS with respect to present day

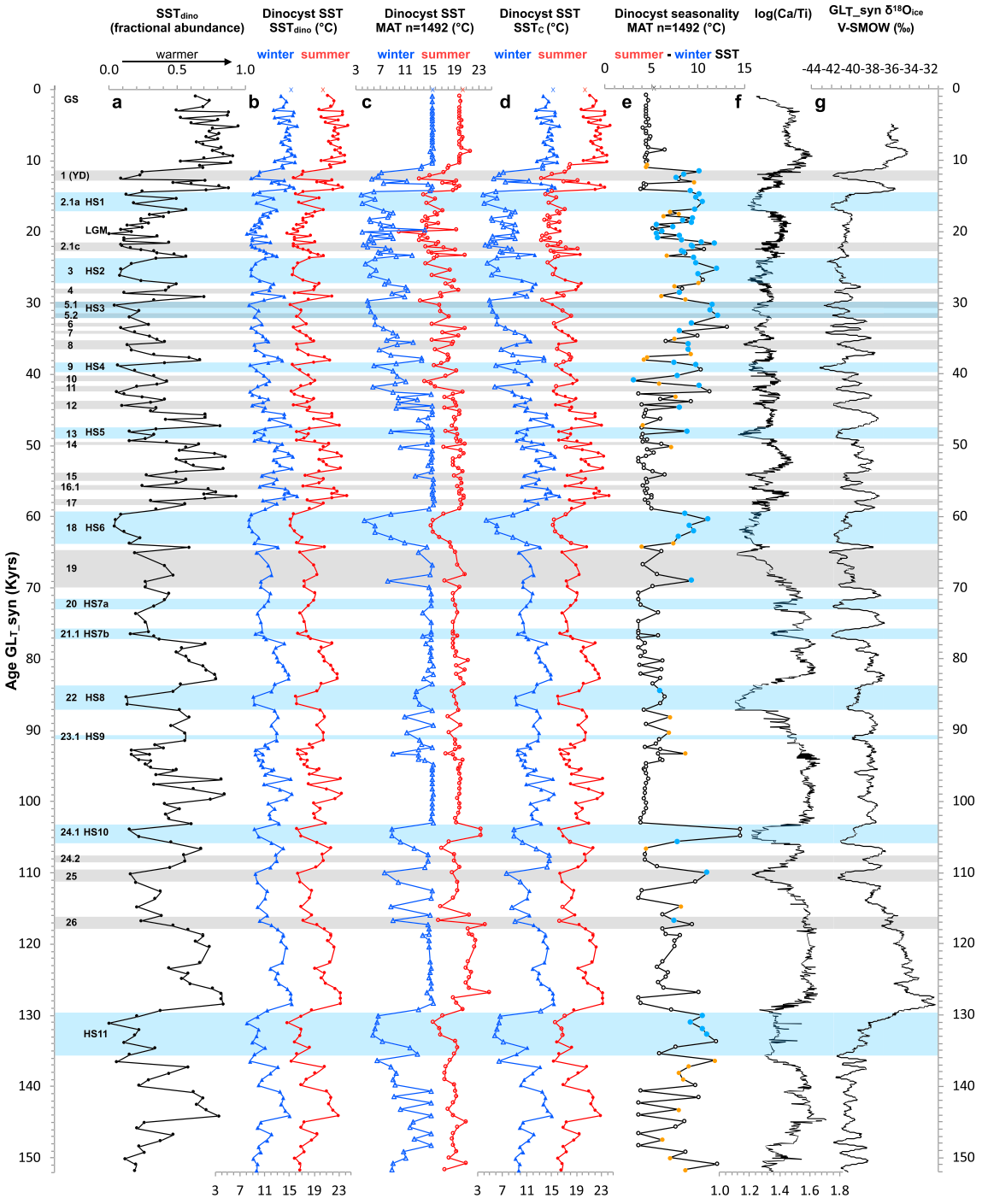

Figure 2. Dinocyst-based sea surface temperature (SST) records and log (Ca/Ti) from Site U1385 encompassing the full last glacial-interglacial cycle. (a) SST_{dino} index of warm versus cold dinocysts (section 3.4.1). (b) Quantified SST_{dino} summer (red circles) and winter (blue triangles) SST (section 3.4.2). (c) Dinocyst modern analog technique (MAT)-based summer and winter SST (section 3.4.3). (d) Composite dinocyst summer and winter SST from the quantified SST_{dino} (closed symbols) and SST_{MAT} (open symbols) (section 3.4.4). (e) Difference between dinocyst MAT-based summer and winter SST (seasonality). Orange and blue circles indicate values that are used to calculate seasonality for warm and cold intervals, respectively. Open circles indicate the values that are disregarded, because summer and/or winter MAT SST reached its limit (section 3.4.3). (f) Log (Ca/Ti) of the AB splice (Hodell et al., 2015). (g) Greenland synthetic $\delta^{18}O$ temperature (Barker et al., 2011). All data in (a)–(f) are from Site U1385 and are placed on our improved GL_T_syn (Speleo-Age) (section 3.2). Crosses at 0 ka indicate present-day values. Gray and blue shades represent Greenland and Heinrich stadials. For the definition and numbering of Greenland Stadials and Interstadials (GS and GI) we follow the updated INTIMATE event stratigraphy of Rasmussen et al. (2014). For the numbering of HS we follow Guillevic et al. (2014). We take the Last Glacial Maximum as the interval between the end of HS2 and the start of HS1 (corresponding to ~23–18 ka on the GLT_syn age model), following Mix et al. (2001). YD = Younger Dryas; HS = Heinrich Stadials.

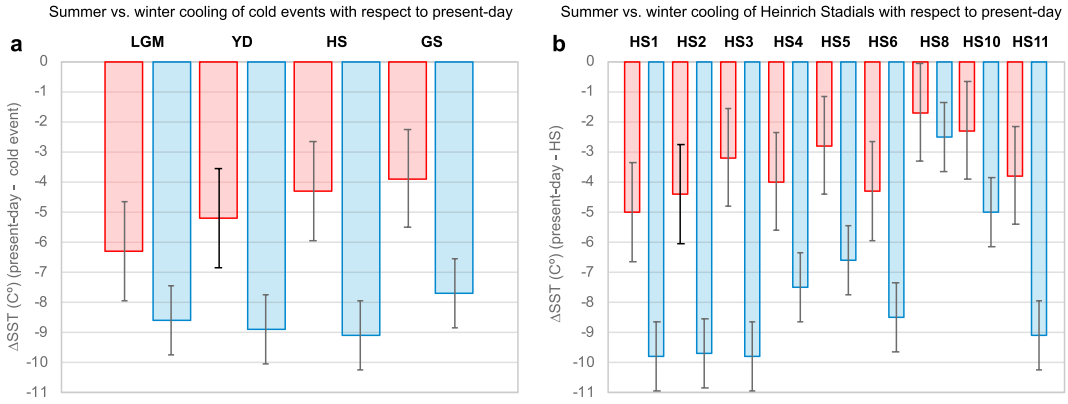

Figure 3. Seasonality during cold events at Site U1385. Difference in summer (red) and winter (blue) SST with respect to the present day (summer: 20.4 °C, winter: 15.3 °C) for several cold events at Site U1385 calculated from dinocyst MAT-based SSTs (excluding all values above the limits of the MAT (section 3.4.3). The values for the LGM, YD, HS, and stadials are average values calculated from all data points in the respective intervals. Since HEs are defined based on the presence of IRD and IRD is only present along the WIM for HS1-6 (de Abreu et al., 2003; Salgueiro et al., 2010), only HS1-6 are included in the HS category in (a). The Greenland Stadials (GS) category represents all other stadials (including HS7-11). Error bars indicate the error of prediction of the MAT (Section 3.4.3). SST = sea surface temperature; MAT = modern analog technique; LGM = Last Glacial Maximum; YD = Younger Dryas; HS = Heinrich Stadials; IRD = ice rafted debris; WIM = West Iberian Margin.

are significantly less than some of the more recent HS (and HS11), which is consistent with the general cooling trend of the glacial cycle.

5. Discussion

Seasonality is likely to have changed in concert with climate shifts, potentially with even larger amplitudes than at present day as one season might be affected more than the other (IPCC, 2013). How changes in seasonality vary regionally and with latitude can be studied with MAT-based approaches. Here we added a new dinocyst MAT-based record of SST seasonality from the WIM to contribute to our understanding of the seasonal component of millennial-scale climate variability during the full last glacial cycle.

5.1. Dinocyst Assemblage-Based Seasonality: Limits and Advantages

Our reconstructions of SST seasonality are based on the MAT applied to dinocyst assemblages, which assumes that similar assemblages are likely to occur under similar conditions. However, multiple factors contribute to the total composition of the assemblages: along with SST and sea ice, salinity and productivity are important (e.g., de Vernal, Hillaire-Marcel, et al., 2013; de Vernal, Rochon, et al., 2013). Zonneveld et al. (2013) showed that SST explains most (~40%) of the variation in the distribution of dinocyst assemblages in present-day samples, suggesting that SST is the main variable driving their distribution on a global scale. The driving factor of dinoflagellate assemblages might actually change over time, but the generally good comparison of our dinocyst-based MAT SSTs with different published SSTs records from Greenland and the WIM (Figure 2 and section 5.2.1) confirms that dinocyst-based MAT SST reconstructions are robust. However, the WIM is an upwelling area and for periods in which productivity was potentially high due to upwelling reconstructed SSTs might be too warm (sections 2 and 3.4.4 and Figure S3). For example, during the Late Holocene and during MIS 5c during which a relatively high abundance of *Lingulodinium machaerophorum* (Figure S4) is indicative of upwelling along the WIM (Ribeiro et al., 2016; Ribeiro & Amorim, 2008). Another variable likely to have a major impact is seasonality, which at present strongly impacts plankton (e.g., Haug et al., 2005; Schiebel & Hemleben, 2005; Schneider et al., 2010; Tierney & Tingley, 2018).

SSTs from dinocyst-based MAT could be biased by changes in the growing season of dinoflagellates through time. To further investigate this, we analyzed the relation between summer and winter in the present-day North Atlantic using the analog reference data set (de Vernal, Hillaire-Marcel, et al., 2013; de Vernal, Rochon, et al., 2013) and compared it with the relation through time between reconstructed summer and winter time series. In the modern reference data set, summer and winter SSTs positively correlate (R^2 = 0.8) despite a large scatter of values up to 18 °C with mean and standard deviation of 6.5 ± 3.7 °C. The reconstructed temporal relation between dinocyst MAT summer and winter is characterized by a lower

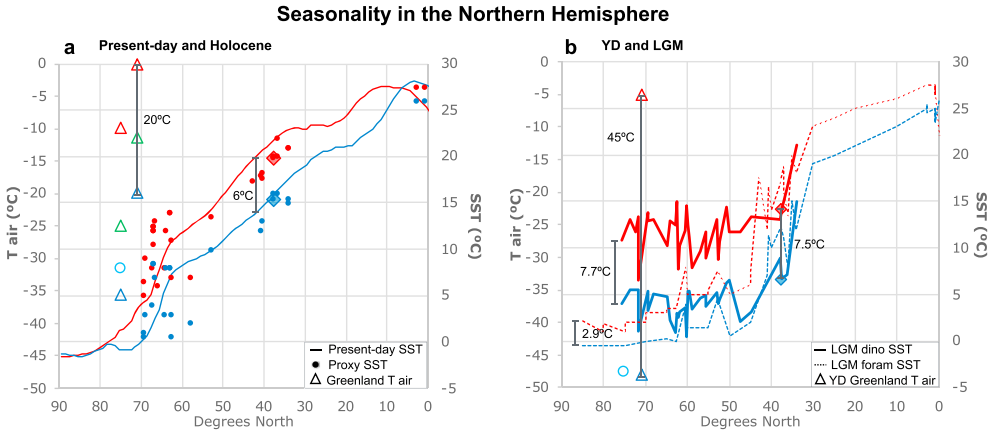

Figure 4. Seasonality in the Northern *H*emisphere for (*a*) the present day and Holocene and (*b*) the YD and LGM. Summer (red) and winter (blue) SST (right axis) and Greenland air temperature (left axis) for (a) the present day (solid line for SST and open triangles for *T* air) and the Holocene (closed symbols) and (b) the YD (open symbols) and LGM (lines). (a) Data for the present day were derived from the World Ocean Database (Boyer et al., 2013) and represent zonal averaged SST from 6 to 30°W per latitude. Closed diamonds indicate dinocyst MAT-based Holocene SSTs from Site U1385 (this study). Proxy data for the Holocene represent SSTs from foraminifera (Andersson et al., 2010; Chabaud et al., 2014; Kandiano & Bauch, 2003; Mix et al., 1986; Penaud et al., 2010; Risebrobakken et al., 2003; Salgueiro et al., 2014; Voelker & de Abreu, 2011; Waelbroeck et al., 1998; Wary et al., 2017), diatoms (Berner et al., 2011; Birks & Koç, 2002; Koc et al., 1990; Koc et al., 1992; Koc et al., 1993), radiolarians (Cortese et al., 2005; Dolven et al., 2002), and dinocysts (Penaud et al., 2010; van Nieuwenhove et al., 2016; Wary et al., 2017). Open triangles represent summer, winter, and mean annual (green) air temperature (Harris et al., 2014) and mean annual borehole temperature (open circle, NGRIP Members, 2004) for the NGRIP Site (75°N) and Scoresby Sund (71°N). (b) Diamonds indicate dinocyst MAT-based LGM SSTs from Site U1385 (this study). Solid lines represent dinocyst MAT-based LGM SST (de Vernal et al., 2005; Penaud et al., 2010; Wary et al., 2015, 2017). Dashed lines represent foraminifer MAT-based SST (Kandiano & Bauch, 2003; Pérez-Folgado et al., 2002; Pflaumann et al., 2003; Waelbroeck et al., 1998 (GLAMAP); Penaud et al., 2010; Penaud, Eynaud, Voelker, et al., 2011; Salgueiro et al., 2014; Voelker & de Abreu, 2011; Wary et al., 2015, 2017) and foraminifer $\delta^{18}O_{Nps}$-based SST (Meland et al., 2005). Open triangles represent summer, winter, and mean annual air temperature at Scoresby Sund (71°N) for the YD (Broecker, 2006; Denton et al., 2005) and mean annual borehole temperature for the NGRIP Site (75°N) (Kindler et al., 2014; Severinghaus et al., 1998). SST = sea surface temperature; YD = Younger Dryas; LGM = Last Glacial Maximum.

correlation coefficient ($R^2 = 0.58$), which implies changes in seasonality over time. When considering the values of the selected analogs, the coefficient of correlation is even lower ($R^2 = 0.49$), which indicates that the calculation of the weighted average yielding the reconstructed value probably smooths the signal. Moreover, the seasonal gradient is not just randomly lower or higher, but systematically higher during cold periods (Figures 2e and 3).

We based our seasonality calculations on dinocyst-based MAT. We observe that the MAT has its limits, due to the reference database, but this mainly affects the reconstruction of the warmer intervals (Figure 2e and section 3.4.3). This is why we limit ourselves to calculate seasonality for the colder intervals and consider the estimates for the warmer intervals as minimum values. Moreover, for all calculated intervals, we left out the data points where the MAT was at its limit due to distant analogs. There could, however, be a small effect of the upper MAT limit in attenuating seasonality derived from dinocyst MAT, because also in some of the cold intervals the MAT has some values close to this limit. Still, for these intervals the reconstructed MAT SSTs correspond quite well to other SST reconstructions, suggesting that MAT results here are quite robust.

5.2. Seasonality in the North Atlantic During the Last Glacial Cycle

5.2.1. Proxy Carriers and Regional Variability

We observed increased seasonality in SST at Site U1385 during the glacial cycle (8.3 °C on average, 9.0 °C for cold events), with respect to present day (5.1 °C) at the WIM. At present day, the average seasonality (summer-winter SST) in the North Atlantic (from 6–30°W) ranges from a minimum of 0 °C at the equatorial latitudes to a maximum of 6 °C at 40°N (Figure 4a). Average seasonality decreases to 0 °C again toward the highest latitudes, because minimum SSTs do not drop below −2 °C. The lowest seasonality observed at Site U1385 during the glacial cycle (3–5 °C) corresponds to the maximum average seasonality observed in

the North Atlantic today, at midlatitudes. Seasonality >6 °C (with a maximum of 8.6 °C) is rarely observed in the North Atlantic (from 6–30°W), only at ~66°N (Iceland) and ~15°N (West Africa) (World Ocean Database: Boyer et al., 2013). Seasonality (summer-winter SST) calculated from dinocyst MAT-based SST at Site U1385 indicates seasonality beyond this present-day maximum (up to 12.2 °C) in a large part of the glacial cycle, with increasing seasonality in MIS 3-2 (Figure 2).

For equatorial latitudes of the North Atlantic (0–10°N, 10–30°W) foraminiferal MAT-based seasonality shows the same seasonal contrast (0–2 °C) in interglacial stages (MIS 1, MIS 5e) as present day (Figure 4a) and at most a somewhat increased seasonality (1.5–6 °C) in cold intervals (YD, LGM, end of MIS 3, MIS 2, and MIS 6) (Figure 4b; Mix et al., 1986; Meland et al., 2005; Pflaumann et al., 2003; Sarnthein et al., 2003; Waelbroeck et al., 1998). For a few sites off West Africa (~20°N) seasonality of 7–8 °C (for MIS 1) and 6–9 °C (for the LGM) are reconstructed (Mix et al., 1986; Pflaumann et al., 2003), but seasonality is similarly high at these locations as present day, which is likely related to upwelling that is more persistent at this location than off the WIM. Increased seasonality in cold glacial intervals, albeit rather limited, is mainly related to lower winter SSTs (Waelbroeck et al., 1998).

For the midlatitudes (37–53°N), including the WIM, seasonality reconstructed based on foraminiferal census data over the full glacial cycle (~3–5 °C) is the same as present day, with no substantial changes between glacials (MIS 6, MIS 5d to MIS 2, LGM: Figure 4b), interglacials (MIS 5e, MIS 1), (Heinrich) stadials and interstadials (Kandiano & Bauch, 2003; Penaud et al., 2010; Pflaumann et al., 2003; Voelker & de Abreu, 2011; Waelbroeck et al., 1998). In contrast to foraminifera-based records, dinocysts suggested much higher seasonal contrasts (~4–12 °C) in the North Atlantic (0–30°W) during the LGM (Figure 4b; de Vernal et al., 2005). Along the WIM (Site MD95-2042), dinocyst-based reconstructions indicate a higher seasonal contrast (~8 °C) for MIS 3 and for (Heinrich) stadials (~9 °C) compared to interstadials (~7 °C; Penaud, Eynaud, Sanchez Goñi, et al., 2011). The large change in seasonal contrast in these dinocyst-based reconstructions is mainly due to extremely low winter SSTs recorded during these cold intervals (Figure 4b; de Vernal et al., 2005; Penaud, Eynaud, Sanchez Goñi, et al., 2011). Such a strong decrease in winter temperatures was suggested earlier by Combourieu-Nebout et al. (2002) and Penaud, Eynaud, Sanchez Goñi, et al. (2011) for (Heinrich) stadials in the Alboran Sea, albeit for the time interval spanning 50 ka to recent. Our dinocyst MAT-based SST reconstructions of Site U1385 are in line with these published dinocyst data (Figures 2 and 4b).

In southwestern Europe (France and Iberian Peninsula), increased seasonality in surface air temperatures is reconstructed for cold episodes based on model results and paleo-ecological reconstructions mainly due to extremely low winter temperatures. During the LGM drops in summer temperature of 0–3 °C are reconstructed compared to present day (Wu et al., 2007), while winter temperatures decrease by 8–17 °C based on vegetation models (Wu et al., 2007), by 5–25 °C based on high-resolution atmospheric models (Jost et al., 2005) and by 15–30 °C according to pollen-based MAT estimates (Peyron et al., 1998). During GS1 and GS2, a decrease in summer temperature of 0–5 °C with respect to present day is reconstructed from pollen and chironomids using MAT (Peyron et al., 2005, and references therein) and 1–5 °C from a compilation of paleo-ecological data (Renssen & Isarin, 2001), whereas a decrease of 10–14 °C in winter temperature is estimated from the compilation of paleo-ecological data (Renssen & Isarin, 2001). Van Meerbeeck et al. (2011) simulated 5–8 °C colder summer temperatures and 8–17 °C colder winter temperatures for GS15 compared to GI14 over southwestern Europe, which is in reasonable agreement with reconstructed climatic and vegetation changes on the Iberian Margin and in France (e.g., Sanchez Goñi et al., 2008). This increased seasonality in southwestern Europe as result of mainly lower winter temperatures is in line with the larger seasonal contrast observed from dinocysts along the WIM.

At present, seasonality increases with latitude. Seasonality in air temperature over the North Atlantic increases from 0 °C at the equator to 40 °C at 90°N (NCEP/NCAR Reanalysis), with very cold winters (−35 °C) over Greenland (Figure 4a). Colder atmospheric temperatures and the presence of sea ice and continental ice sheets at higher latitudes suppress the influence of the maritime climate as is found at the midlatitudes, Hence, it is expected that during past cooling events, winters were even colder at high latitudes. Flückiger et al. (2008) indeed simulated the strongest change in surface air temperature in the North Atlantic region between GS and GI in winter, increasing with latitude from 0 °C at the equator to 30 °C near Greenland. Surface annual air temperature at the NGRIP site (Greenland), reconstructed from ice core air

$\delta^{15}N$ was 16 °C colder during cold events of the last glacial cycle with respect to present-day borehole temperature at the site (−31.5 °C; Severinghaus et al., 1998; Guillevic et al., 2013; Kindler et al., 2014; Kobashi et al., 2017; Tabone et al., 2018). Such a temperature drop is also observed during the YD (Figure 4b; Severinghaus et al., 1998; Kindler et al., 2014), whereas glacier evidence from Eastern Greenland suggests a cooling of only ~5–10 °C during the summer (Broecker, 2006; Denton et al., 2005; Lie & Paasche, 2006). Broecker (2006) suggested that the combined data requires a hypothetical 28 °C winter cooling during the YD over Greenland, resulting in a seasonal contrast of 45 °C at Scoresby Sund, which is more than double today's value (Figure 4b).

Based on literature review, Denton et al. (2005) have shown a similar and consistent picture for the YD in northern and central Europe, with reconstructed drops in summer temperatures of only 3–7 °C based on fossil beetles (Atkinson et al., 1987), pollen and plants (Isarin & Bohncke, 1997), chironomids (Brooks et al., 1997; Brooks & Birks, 2001), and equilibrium-line altitude depression (Dahl & Nesje, 1992). Reconstructed drops in mean annual temperature are 12–17 °C and 22 °C for winter temperature based on periglacial features (Denton et al., 2005; Isarin et al., 1998; Isarin & Renssen, 1999). Moreover, for the LGM and stadials of MIS 3, increased seasonality due to severe drops in winter temperature was reconstructed across the North Atlantic based on ice rafted debris (IRD), moraine and ice core records (Denton et al., 2005, and references therein). Obviously, this large seasonal contrast would be dampened in SST, not only due to the large heat capacity of water but also due to the minimum temperature of liquid seawater of ~ −1.8 °C prior to freezing. Still, at subpolar latitudes a major decrease in winter SST would be expected during such extreme cold events.

Present-day seasonality in SST at the higher latitudes (60–75°N) is only 3.4 °C (Figure 4a). MAT-based SSTs and seasonality (5 °C) from dinocysts, foraminifera, and diatoms are slightly higher, but comparable to present day in MIS 1. Limited available seasonal data based on diatom MAT suggest that seasonality was not increased at these latitudes in the YD (3.9 °C, Birks & Koç, 2002; Koc et al., 1992; Koc et al., 1993), during the LGM based on foraminiferal MAT (2.9 °C, Pflaumann et al., 2003; 4 °C, Wary et al., 2015, 2017; Figure 4b), and from GS10-5 based on foraminiferal MAT (4 °C, Wary et al., 2015, 2017). In contrast, dinocyst MAT-based SSTs indicate increased seasonality at higher latitudes relative to the present day during the LGM (7.7 °C, de Vernal et al., 2005; 12–14 °C, Wary et al., 2015, 2017; Figure 4b) and GS10-5 (~12–14 °C, Wary et al., 2015, 2016, 2017, 2018).

Overall, dinocyst assemblages led to reconstruct higher seasonality during past cold events than diatoms and foraminifera. Jonkers and Kucera (2017) demonstrated that temperature and associated environmental changes cause shifts in seasonal and depth habitat of planktonic foraminifera, which may lead to pronounced dampening in the amplitude of recorded environmental change. They calculated up to 40% reduction in temperature gradients, both in space and time. In addition, the dinocyst-based reconstructions of SST are more in line with reconstructed and modeled seasonality from the European continent. Hence, foraminifera probably underestimate seasonality (see also the discussion in Datema et al. (2017)). Here we provide evidence that the difference in reconstructed summer and winter SSTs is consistent in the North Atlantic, and we show that over longer time scales increased seasonality remains linked to the colder phases of the glacial cycle.

5.2.2. Mechanisms of Increased Cold Climate Seasonality

Our data suggest that seasonality during HS was larger compared to the LGM and YD (Figure 3a). Although the difference is not statistically significant in our data, this is in line with the conclusions of Cacho et al. (1999) and Rahmstorf (2002), who also showed more cooling during HS than that observed for stadials for the more southern North Atlantic and Alboran Sea. Denton et al. (2005) showed that stadials mainly reflect winter cooling, whereas the LGM involved much summertime cooling as well. Our results confirm this indirect inference through actual summer and winter temperature reconstructions. Milankovitch's theory states that on orbital time scales northern summer insolation drives important processes such as monsoon activity and ice sheet dynamics (Berger, 1978; Ruddiman, 2003). For the abrupt winter-dominated millennial time scale events several mechanisms have been proposed, including sea ice variability (Gildor & Tziperman, 2003; Li et al., 2005), ice shelf growth and decay (Petersen et al., 2013), shifts in preferred Northern Hemisphere planetary wave patterns (Seager & Battisti, 2007; Wunsch, 2006), and orbitally driven SST changes in the tropics (Clement et al., 2001). An often-invoked explanation for the abrupt millennial scale climate changes is the hypothesis of changes in the Atlantic meridional overturning circulation

(AMOC) and resulting changes in the extent of North Atlantic sea ice (Broecker et al., 1985; Clark et al., 2002; Lynch-Stieglitz, 2017; Rahmstorf, 2002).

Changes in strength and structure of the AMOC could have contributed to the large impact of winters in seasonality switches between stadials and interstadials. During the YD, LGM, stadials, and HS rerouting of meltwater input from ice sheets and/or meltwater lakes might have caused shutdown of the AMOC, with, as a consequence, a decrease in northward oceanic heat transport. This in turn would have allowed the formation of extensive winter sea ice cover in the North Atlantic, resulting in a continental climate type throughout Europe and particularly colder winters, hence increased seasonality (Broecker, 2006; Denton et al., 2005; Flückiger et al., 2008; Jost et al., 2005; Lynch-Stieglitz, 2017; Rahmstorf, 2002; Renssen & Isarin, 2001; Sarnthein et al., 2003; Van Meerbeeck et al., 2011). Dinoflagellate populations depend upon parameters linked to sea ice cover, such as increased seasonality and lower salinity and temperature. The fact that HS are associated with a stronger increase in seasonality during colder periods of the glacial stages than the warmer periods (Figure 3b), supports this sea ice scenario. At Site U1385, SST indeed decreases during cold (Heinrich) events (Figures 2b–2e), which is in line with a slowdown in the thermohaline circulation. In addition, IRD has been observed at sites MD99-2334 and SU81-18 close to Site U1385 (Figure 1) during the YD and HS1-3 (Bard et al., 2000; Skinner & Shackleton, 2004). Also $C_{37:4}$ alkenone data indicate the presence of low-salinity water masses at sites SU81-18 and MD01-2444 coincident with these IRD events (Bard et al., 2000; Martrat et al., 2007). Hence, it is likely that sea ice advanced more toward the south influencing the oceanographic conditions at the southern WIM during cold events. There is clear evidence that there were significant changes in the AMOC associated with the LGM, YD, some HS, and D-O events; however, the relation between freshwater input, AMOC changes, and climate changes is not yet fully understood for HS and DO events (Lynch-Stieglitz, 2017).

6. Conclusions

We present here reconstructions of millennial-scale variability in summer and winter SST based on dinoflagellate cyst assemblages, thereby combining qualitative and quantitative (MAT) approaches, from the WIM (IODP Shackleton Site U1385) over the last 152 kyrs. This allowed the investigation of the role of seasonality in rapid (Dansgaard-Oeschger and Heinrich) climate shifts. Our dinocyst SST tracers show the rapid climate shifts related to the D-O and Heinrich (inter)stadials and correlate to these same events from the Greenland ice core records. The MAT summer and winter temperatures imply a seasonality that reproduces the modern value for MIS 1 (~5 °C) and shows that seasonality increased to up to 12 °C during the cold events of the glacial cycle, mainly due to strong winter cooling. Our temperature and seasonality reconstructions are in line with previously published data that show increased seasonality due to strong winter cooling during the YD and LGM for the European continent and North Atlantic region. We show that increased seasonality remains linked to the colder phases of the glacial cycle also over longer time scales. This is particularly evident during HS. Changes in the strength and structure of the AMOC and formation of extensive winter sea ice cover in the North Atlantic could have contributed to the large impact of winters in seasonality switches between stadials and interstadials.

Acknowledgments
This work used samples and data provided by the Integrated Ocean Drilling Program (IODP). We thank Walter Hale and Alex Wülbers from the IODP Core Repository in Bremen for curation of the sediment cores recovered at Site U1385. We acknowledge all shipboard participants of IODP Expedition 339 and particularly David Hodell for providing the age models. We thank Natasja Welters (Utrecht University) for laboratory assistance. We gratefully acknowledge the reviewers for their thoughtful comments that helped us to greatly improve this manuscript. The European Research Council (ERC) under the European Union Seventh Framework Program provided funding for this work by ERC Starting grant 259627 to Sluijs. This work was carried out under the program of the Netherlands Earth System Science Centre (NESSC). Our data can be found online as supporting information to this publication.

References

Andersson, C., Pausata, F. S. R., Jansen, E., Risebrobakken, B., & Telford, R. J. (2010). Holocene trends in the foraminifer record from the Norwegian Sea and the North Atlantic Ocean. *Climate of the Past*, *6*(2), 179–193. https://doi.org/10.5194/cp-6-179-2010

Arístegui, J., Álvarez-Salgado, X. A., Barton, E. D., Figueiras, F. G., Hernández-León, S., Roy, C., & Santos, A. M. P. (2005). Chapter 23: Oceanography and fisheries of the Canary Current/Iberian region of the eastern North Atlantic (18a, E). In K. H. Brink & A. R. Robinson (Eds.), *The sea : the global coastal ocean : interdisciplinary regional studies and syntheses* (Vol. 14, pp. 877–931). Harvard: Harvard University Press. ISBN 0-674-01527-4

Arístegui, J., Barton, E. D., Álvarez-Salgado, X. A., Santos, A. M. P., Figueiras, F. G., Kifani, S., et al. (2009). Sub-regional ecosystem variability in the Canary Current upwelling. *Progress in Oceanography*, *83*(1-4), 33–48. https://doi.org/10.1016/j.pocean.2009.07.031

Atkinson, T. C., Briffa, K. R., & Coope, G. R. (1987). Seasonal temperatures in Britain during the past 22.000 years, reconstructed using beetle remains. *Nature*, *325*(6105), 587–592. https://doi.org/10.1038/325587a0

Bard, E., Rostek, F., Turon, J.-L., & Gendreau, S. (2000). Hydrological impact of Heinrich events in the subtropical Northeast Atlantic. *Science*, *289*(5483), 1321–1324. https://doi.org/10.1126/science.289.5483.1321

Barker, S., Knorr, G., Edwards, R. L., Parrenin, F., Putnam, A. E., Skinner, L. C., et al. (2011). 800,000 years of abrupt climate variability. *Science*, *334*(6054), 347–351. https://doi.org/10.1126/science.1203580

Beck, J. W., Edwards, R. L., Ito, E., Taylor, F. W., Recy, J., Rougerie, F., et al. (1992). Sea-surface temperature from coral skeletal Strontium/Calcium ratios. *Science*, *257*(5070), 644–647. https://doi.org/10.1126/science.257.5070.644

Berger, A. (1978). Long-term variations of caloric insolation resulting from the earth's orbital elements. *Quaternary Research*, *9*(02), 139–167. https://doi.org/10.1016/0033-5894(78)90064-9

Berner, K. S., Koç, N., Godtliebsen, F., & Divine, D. (2011). Holocene climate variability of the Norwegian Atlantic Current during high and low solar insolation forcing. *Paleoceanography*, *26*, PA2220. https://doi.org/10.1029/2010PA002002

Birks, C. J., & Koç, N. (2002). A high-resolution diatom record of late-Quaternary sea-surface temperatures and oceanographic conditions from the eastern Norwegian Sea. *Boreas*, *31*(4), 323–344. https://doi.org/10.1111/j.1502-3885.2002.tb01077.x

Boyer, T. P., Antonov, J. I., Baranova, O. K., Coleman, C., Garcia, H. E., Grodsky, A., et al. (2013). In S. Levitus, & A. Mishonov (Eds.), *World ocean database 2013*, NOAA Atlas NESDIS (Vol. *72*, p. 209). Silver Spring, MD: National Oceanographic Data Center Ocean Climate Laboratory. https://doi.org/10.7289/V5NZ85MT, http://odv.awi.de/en/data/ocean/world_ocean_atlas_2013/

Broecker, W. S. (2006). Abrupt climate change revisited. *Global and Planetary Change*, *54*(3-4), 211–215. https://doi.org/10.1016/j.gloplacha.2006.06.019

Broecker, W. S., Peteet, D. M., & Rind, D. (1985). Does the ocean–atmosphere system have more than one stable mode of operation? *Nature*, *315*(6014), 21–26. https://doi.org/10.1038/315021a0

Brooks, S. J., & Birks, H. J. B. (2001). Chironomid-inferred air temperatures from Lateglacial and Holocene sites in north-west Europe: progress and problems. *Quaternary Science Reviews*, *20*(16-17), 1723–1741. https://doi.org/10.1016/S0277-3791(01)00038-5

Brooks, S. J., Mayle, F. E., & Lowe, J. J. (1997). Chironomid-based Lateglacial climatic reconstruction for southeast Scotland. *Journal of Quaternary Science*, *12*(2), 161–167. https://doi.org/10.1002/(SICI)1099-1417(199703/04)12:2<161::AID-JQS303>3.0.CO;2-T

Cacho, I., Grimalt, J. O., Pelejero, C., Canals, M., Sierro, F. J., Flores, J. A., & Shackleton, N. (1999). Dansgaard-Oeschger and Heinrich event imprints in Alboran Sea paleotemperatures. *Paleoceanography*, *14*(6), 698–705. https://doi.org/10.1029/1999PA900044

Carré, M., & Cheddadi, R. (2017). Seasonality in long-term climate change. *Quaternaire*, *28*(2), 173–177.

Cayre, O., Lancelot, Y., & Vincent, E. (1999). Paleoceanographic reconstructions from planktonic foraminifera off the Iberian Margin: temperature, salinity, and Heinrich events. *Paleoceanography*, *14*(3), 384–396. https://doi.org/10.1029/1998PA900027

Chabaud, L., Sánchez Goñi, M. F., Desprat, S., & Rossignol, J. (2014). Land–sea climatic variability in the eastern North Atlantic subtropical region over the last 14,200 years: Atmospheric and oceanic processes at different timescales. *The Holocene*, *24*(7), 787–797. https://doi.org/10.1177/0959683614530439

Clark, P. U., Pisias, N. G., Stocker, T. F., & Weaver, A. J. (2002). The role of the thermohaline circulation in abrupt climate change. *Nature*, *415*(6874), 863–869. https://doi.org/10.1038/415863a

Clement, A. C., Cane, M. A., & Seager, R. (2001). An orbitally driven tropical source for abrupt climate change. *Journal of Climate*, *14*(11), 2369–2375. https://doi.org/10.1175/1520-0442(2001)014<2369:AODTSF>2.0.CO;2

Combourieu-Nebout, N., Turon, J. L., Zahn, R., Capotondi, L., Londeix, L., & Pahnke, K. (2002). Enhanced aridity and atmospheric high-pressure stability over the western Mediterranean during the North Atlantic cold events of the past 50 k.y. *Geology*, *30*(10), 863–866. https://doi.org/10.1130/0091-7613(2002)030<0863:EAAAHP>2.0.CO;2

Corège, T., Gagan, M. K., Beck, J. W., Burr, G. S., Cabioch, G., & Le Cornec, F. (2004). Interdecadal variation in the extent of South Pacific tropical waters during the Younger Dryas event. *Nature*, *428*(6986), 927–929. https://doi.org/10.1038/nature02506

Cortese, G., Dolven, J. K., Bjørklund, K. R., & Malmgren, B. A. (2005). Late Pleistocene–Holocene radiolarian paleotemperatures in the Norwegian Sea based on artificial neural networks. *Palaeogeography, Palaeoclimatology, Palaeoecology*, *224*(4), 311–332. https://doi.org/10.1016/j.palaeo.2005.04.015

Dahl, S. O., & Nesje, A. (1992). Paleoclimatic implications based on equilibrium-line altitude depressions of reconstructed Younger Dryas and Holocene cirque glaciers in Inner Nordfjord, Western Norway. *Palaeogeography Palaeoclimatology Palaeoecology*, *94*(1-4), 87–97. https://doi.org/10.1016/0031-0182(92)90114-K

Datema, M., Sangiorgi, F., de Vernal, A., Reichart, G.-J., Lourens, L. J., & Sluijs, A. (2017). Comparison of qualitative and quantitative dinoflagellate cyst approaches in reconstructing glacial-interglacial climate variability at West Iberian Margin IODP 'Shackleton' Site U1385. *Marine Micropaleontology*, *136*, 14–29. https://doi.org/10.1016/j.marmicro.2017.08.003

de Abreu, L., Shackleton, N. J., Schönfeld, J., Hall, M., & Chapman, M. (2003). Millennial-scale oceanic climate variability of the Western Iberian margin during the last two glacial periods. *Marine Geology*, *196*(1-2), 1–20. https://doi.org/10.1016/S0025-3227(03)00046-X

de Vernal, A., Eynaud, F., Henry, M., Hillaire-Marcel, C., Londeix, L., Mangin, S., et al. (2005). Reconstruction of sea-surface conditions at middle to high latitudes of the Northern Hemisphere during the Last Glacial Maximum (LGM) based on dinoflagellate cyst assemblages. *Quaternary Science Reviews*, *24*(7-9), 897–924. https://doi.org/10.1016/j.quascirev.2004.06.014

de Vernal, A., Henry, M., Matthiessen, J., Mudie, P. J., Rochon, A., Boessenkool, K. P., et al. (2001). Dinoflagellate cyst assemblages as tracers of sea-surface conditions in the northern North Atlantic, Arctic and sub-Arctic seas: The new "$n = 677$" database and its application for quantitative palaeoceanographic reconstruction. *Journal of Quaternary Science*, *16*(7), 681–698. https://doi.org/10.1002/jqs.659

de Vernal, A., Rochon, A., Fréchette, B., Henry, M., Radi, T., & Solignac, S. (2013). Reconstructing past sea ice cover of the Northern Hemisphere from dinocyst assemblages: Status of the approach. *Quaternary Science Reviews*, *79*, 122–134. https://doi.org/10.1016/j.quascirev.2013.06.022

de Vernal, A., Hillaire-Marcel, C., Rochon, A., Fréchette, B., Henry, M., Solignac, S., & Bonnet, S. (2013). Dinocyst-based reconstructions of sea ice cover concentration during the Holocene in the Arctic Ocean, the northern North Atlantic Ocean and its adjacent seas. *Quaternary Science Reviews*, *79*, 111–121. https://doi.org/10.1016/j.quascirev.2013.07.006

de Vernal, A., Hillaire-Marcel, C., Turon, J.-L., & Matthiessen, J. (2000). Reconstruction of sea-surface temperature, salinity, and sea-ice cover in the northern North Atlantic during the last glacial maximum based on dinocyst assemblages. *Canadian Journal of Earth Sciences*, *37*(5), 725–750. https://doi.org/10.1139/e99-091

de Vernal, A., Rosell-Melé, A., Kucera, M., Hillaire-Marcel, C., Eynaud, F., Weinelt, M., et al. (2006). Comparing proxies for the reconstruction of LGM sea-surface conditions in the northern North Atlantic. *Quaternary Science Reviews*, *25*(21-22), 2820–2834. https://doi.org/10.1016/j.quascirev.2006.06.006

Denton, G. H., Alley, R. B., Comer, G. C., & Broecker, W. S. (2005). The role of seasonality in abrupt climate change. *Quaternary Science Reviews*, *24*(10-11), 1159–1182. https://doi.org/10.1016/j.quascirev.2004.12.002

Dolven, J. K., Cortese, G., & Bjørklund, K. R. (2002). A high-resolution radiolarian-derived paleotemperature record for the Late Pleistocene-Holocene in the Norwegian Sea. *Paleoceanography*, *17*(4), 1072. https://doi.org/10.1029/2002PA000780

Donnelly, A., & Yu, R. (2017). The rise of phenology with climate change: an evaluation of IJB publications. *International Journal of Biometeorology*, *61*(Suppl 1), S29–S50. https://doi.org/10.1007/s00484-017-1371-8

Eynaud, F.,Londeix, L., Penaud, A., Sanchez-Goni, M.-F., Oliveira, D., Desprat, S., & Turon, J.-L. (2016). Dinoflagellate cyst population evolution throughout past interglacials: Key features along the Iberian margin and insights from the new IODP Site U1385 (Exp 339). *Global and Planetary Change*, *136*, 52–64. https://doi.org/10.1016/j.gloplacha.2015.12.004

Expedition 339 Scientists: Site U1385 (2013). In D. A. V. Stow, F. J. Hernández-Molina, C. A. Alvarez Zarikian, & Expedition 339 Scientists (Eds.), *Proc. IODP* (Vol. 339). Tokyo: Integrated Ocean Drilling Program Management International, Inc. https://doi.org/10.2204/iodp.proc.339.103.2013

Felis, T., Lohmann, G., Kuhnert, H., Lorenz, S. J., Scholz, D., Patzold, J., et al. (2004). Increased seasonality in Middle East temperatures during the last interglacial period. *Nature*, *429*(6988), 164–168. https://doi.org/10.1038/nature02546

Flückiger, J., Knutti, R., White, J. W. C., & Renssen, H. (2008). Modeled seasonality of glacial abrupt climate events. *Climate Dynamics*, *31*(6), 633–645. https://doi.org/10.1007/s00382-008-0373-y

Gildor, H., & Tziperman, E. (2003). Sea-ice switches and abrupt climate change. *Philosophical Transactions of the Royal Society of London. Series A*, *361*(1810), 1935–1944. https://doi.org/10.1098/rsta.2003.1244

Guillevic, M., Bazin, L., Landais, A., Stowasser, C., Masson-Delmotte, V., Blunier, T., et al. (2014). Evidence for a three-phase sequence during Heinrich Stadial 4 using a multiproxy approach based on Greenland ice core records. *Climate of the Past*, *10*(6), 2115–2133. https://doi.org/10.5194/cp-10-2115-2014

Guillevic, M., Bazin, L., Landais, A., Kindler, P., Orsi, A., Masson-Delmotte, V., et al. (2013). Spatial gradients of temperature, accumulation and δ^{18}O-ice in Greenland over a series of Dansgaard-Oeschger events. *Climate of the Past Discussions*, *9*(3), 1029–1051. https://doi.org/10.5194/cp-9-1029-2013

Guiot, J., & de Vernal, A. (2007). Transfer functions: methods for quantitative paleoceanography based on microfossils. In C. Hillaire-Marcel & A. de Vernal (Eds.), *Proxies in Late Cenozoic paleoceanography*, *Developments in Marine Geology* (Vol. 1, pp. 523–563). Amsterdam: Elsevier. https://doi.org/10.1016/S1572-5480(07)01018-4

Harris, I., Jones, P. D., Osborn, T. J., & Lister, D. H. (2014). Updated high-resolution grids of monthly climatic observations – CRU TS3.10: The Climatic Research Unit (CRU) Time Series (TS) Version 3.10 Dataset. *International Journal of Climatology*, *34*(3), 623–642. https://doi.org/10.1002/joc3711; updated to version CRU TS3.24, October 16th, 2016. Climate Change Knowledge Portal, http://sdwebx.worldbank.org/climateportal/

Haug, G. H., Ganopolski, A., Sigman, D. M., Rosell-Mele, A., Swann, G. E. A., Tiedemann, R., et al. (2005). North Pacific seasonality and the glaciation of North America 2.7 million years ago. *Nature*, *433*(7028), 821–825. https://doi.org/10.1038/nature03332

Hodell, D.A., Crowhurst, S., Skinner, L., Tzedakis, P.C., Margari, V., Channell, J.E.T., et al., 2013. Response of Iberian Margin sediments to orbital and suborbital forcing over the past 420 ka. *Paleoceanography 28*, 185–199. https://doi.org/10.1002/palo.20017. (Data at: https://www.ncdc.noaa.gov/paleo/study/15776).

Hodell, D.A., Lourens, L., Crowhurst, S., Konijnendijk, T., Tjallingii, R., Jiménez-Espejo, F., et al., Shackleton Site Project Members, 2015. A reference time scale for Site U1385 (Shackleton Site) on the SW Iberian Margin. *Global and Planetary Change 133*, 49–64. https://doi.org/10.1016/j.gloplacha.2015.07.002. (Data at: https://www.ncdc.noaa.gov/paleo/study/19782).

Hodell, D. A., Lourens, L., Stow, D. A. V., Hernández-Molina, J., Alvarez Zarikian, C. A., & Shackleton Site Project Members (2013). The "Shackleton Site" (IODP Site U1385) on the Iberian Margin. *Scientific Drilling*, *16*, 13–19. https://doi.org/10.5194/sd-16-13-2013

Huybers, P., & Curry, W. (2006). Links between annual, Milankovitch and continuum temperature variability. *Nature*, *441*(7091), 329–332. https://doi.org/10.1038/nature04745

IPCC (2013). Climate Change 2013: The physical science basis. In T. F. Stocker et al. (Eds.), *Contribution of Working Group I to the Fifth Assessment Report of the Intergovernmental Panel on Climate Change* (pp. 1–1535). Cambridge, United Kingdom and New York, NY, USA: Cambridge University Press. http://www.climatechange2013.org

Isarin, R. F. B., & Bohncke, S. J. (1997). Mean July temperatures during the Younger Dryas in northwestern and central Europe as inferred from climate indicator plant species. *Quaternary Research*, *51*, 158–173.

Isarin, R. F. B., & Renssen, H. (1999). Reconstructing and modeling Late Weichselian climates: The Younger Dryas in Europe as a case study. *Earth-Science Reviews*, *48*(1-2), 1–38. https://doi.org/10.1016/S0012-8252(99)00047-1

Isarin, R. F. B., Renssen, H., & Vandenberghe, J. (1998). The impact of the North Atlantic Ocean on the Younger Dryas climate in northwestern and central Europe. *Journal of Quaternary Science*, *13*(5), 447–453. https://doi.org/10.1002/(SICI)1099-1417(1998090)13:5<447::AID-JQS402>3.0.CO;2-B

Jonkers, L., & Kucera, M. (2017). Quantifying the effect of seasonal and vertical habitat tracking on planktonic foraminifera proxies. *Climate of the Past*, *13*(6), 573–586. https://doi.org/10.5194/cp-13-573-2017

Jost, A., Lunt, D., Kageyama, M., Abe-Ouchi, A., Peyron, O., Valdes, P. J., & Ramstein, G. (2005). High-resolution simulations of the last glacial maximum climate over Europe: A solution to discrepancies with continental palaeoclimatic reconstructions? *Climate Dynamics*, *24*(6), 577–590. https://doi.org/10.1007/s00382-005-0009-4

Kandiano, E. S., & Bauch, H. A. (2003). Surface ocean temperatures in the north-east Atlantic during the last 500,000 years: Evidence from foraminiferal census data. *Terra Nova*, *15*(4), 265–271. https://doi.org/10.1046/j.1365-3121.2003.00488.x

Kindler, P., Guillevic, M., Baumgartner, M., Schwander, J., Landais, A., & Leuenberger, M. (2014). Temperature reconstruction from 10 to 120 kyr b2k from the NGRIP Ice Core. *Climate of the Past*, *10*, 887–902. https://doi.org/10.5194/cp-10-887-2014

Kobashi, T., Menviel, L., Jeltsch-Thömmes, A., Vinther, B. M., Box, J. E., Muscheler, R., et al. (2017). Volcanic influence on centennial to millennial Holocene Greenland temperature change. *Nature Scientific Reports*, *7*(1), 1441, 1–1441, 10. https://doi.org/10.1038/s41598-017-01451-7

Koç Karpuz, N., & Jansen, E. (1992). A high-resolution diatom record of the last deglaciation from the SE Norwegian Sea: Documentation of rapid climate changes. *Paleoceanography*, *7*(4), 499–520. https://doi.org/10.1029/92PA01651

Koç Karpuz, N., & Schrader, H. (1990). Surface sediment diatom distribution and Holocene paleotemperature variations in the Greenland, Iceland and Norwegian Seas. *Paleoceanography*, *5*(4), 557–580. https://doi.org/10.1029/PA005i004p00557

Koc, N., Jansen, E., & Haflidason, H. (1993). Paleoceanographic reconstructions of the surface ocean conditions in the Greenland, Iceland and Norwegian Seas throughout the last 14 ka, based on diatoms. *Quaternary Science Reviews*, *12*(2), 115–140. https://doi.org/10.1016/0277-3791(93)90012-B

Kucera, M., Rosell-Mele, A., Schneider, R., Waelbroeck, C., & Weinelt, M. (2005). Multiproxy approach for the reconstruction of the glacial ocean surface (MARGO). *Quaternary Science Reviews*, *24*(7-9), 813–819. https://doi.org/10.1016/j.quascirev.2004.07.017

Lazareth, C. E., Bustamante Rosell, M. G., Turcq, B., Le Cornec, F., Mandeng-Yogo, M., Caquineau, S., & Cabioch, G. (2013). Mid-Holocene climate in New Caledonia (southwest Pacific): coral and PMIP models monthly resolved results. *Quaternary Science Reviews*, *69*, 83–97. https://doi.org/10.1016/j.quascirev.2013.02.024

Li, C., Battisti, D. S., Schrag, D. P., & Tziperman, E. (2005). Abrupt climate shifts in Greenland due to displacements of the sea ice edge. *Geophysical Research Letters*, *32*, L19702. https://doi.org/10.1029/2005GL023492

Lie, O., & Paasche, O. (2006). How extreme was northern hemisphere seasonality during the Younger Dryas? *Quaternary Science Reviews*, *25*(5-6), 404–407. https://doi.org/10.1016/j.quascirev.2005.11.003

Lynch-Stieglitz, J. (2017). The Atlantic meridional overturning circulation and abrupt climate change. *Annual Review of Marine Science*, *9*(1), 83–104. https://doi.org/10.1146/annurev-marine-010816-060415

Martrat, B., Grimalt, J. O., Shackleton, N. J., de Abreu, L., Hutterli, M. A., & Stocker, T. F. (2007). Four climate cycles of recurring deep and surface water destabilizations on the Iberian Margin. *Science*, *317*(5837), 502–507. https://doi.org/10.1126/science.1139994

Meland, M. Y., Jansen, E., & Elderfield, H. (2005). Constraints on SST estimates for the northern North Atlantic/Nordic Seas during the LGM. *Quaternary Science Reviews*, *24*(7-9), 835–852. https://doi.org/10.1016/j.quascirev.2004.05.011

Mix, A. C., Bard, E., & Schneider, R. (2001). Environmental processes of the ice age: Land, oceans, glaciers (EPILOG). *Quaternary Science Reviews*, *20*(4), 627–657. https://doi.org/10.1016/S0277-3791(00)00145-1

Mix, A. C., Ruddiman, W. F., & McIntyre, A. (1986). Late Quaternary paleoceanography of the tropical Atlantic, II: The seasonal cycle of sea-surface temperatures, 0-20,000 years B.P. *Paleoceanography*, *1*(3), 339–353. https://doi.org/10.1029/PA001i003p00339

Morgan, V., & van Ommen, T. D. (1997). Seasonality in late-Holocene climate from ice-core records. *The Holocene*, *7*(3), 351–354. https://doi.org/10.1177/095968369700700312

National Centers for Environmental Prediction/National Weather Service/NOAA/U.S. Department of Commerce. (1994). updated monthly. *NCEP/NCAR global reanalysis products, 1948-continuing*. Research Data Archive at the National Center for Atmospheric Research, Computational and Information Systems Laboratory. http://rda.ucar.edu/datasets/ds090.0/. Accessed 15 Mar 2018.

North Greenland Ice Core Project members (2004). High-resolution record of Northern Hemisphere climate extending into the last interglacial period. *Nature*, *431*(7005), 147–151. https://doi.org/10.1038/nature02805

Peliz, Á., Dubert, J., Santos, A. M. P., Oliveira, P. B., & Le Cann, B. (2005). Winter upper ocean circulation in the Western Iberian basin—Fronts, eddies and poleward flows: An overview. *Deep Sea Research Part I: Oceanographic Research Papers*, *52*(4), 621–646. https://doi.org/10.1016/j.dsr.2004.11.005

Penaud, A., Eynaud, F., Sanchez Goñi, M. F., Malaizé, B., Turon, J. L., & Rossignol, L. (2011). Contrasting sea-surface responses between the western Mediterranean Sea and eastern subtropical latitudes of the North Atlantic during abrupt climatic events of MIS 3. *Marine Micropaleontology*, *80*(1-2), 1–17. https://doi.org/10.1016/j.marmicro.2011.03.002

Penaud, A., Eynaud, F., Turon, J. L., Blamart, D., Rossignol, L., Marret, F., et al. (2010). Contrasting paleoceanographic conditions off Morocco during Heinrich events (1 and 2) and the Last Glacial Maximum. *Quaternary Science Reviews*, *29*(15-16), 1923–1939. https://doi.org/10.1016/j.quascirev.2010.04.011

Penaud, A., Eynaud, F., Voelker, A., Kageyama, M., Marret, F., Turon, J. L., et al. (2011). Assessment of sea surface temperature changes in the Gulf of Cadiz during the last 30 ka: Implications for glacial changes in the regional hydrography. *Biogeosciences*, *8*(8), 2295–2316. https://doi.org/10.5194/bg-8-2295-2011

Pérez, F. F., Castro, C. G., Álvarez-Salgado, X. A., & Ríos, A. F. (2001). Coupling between the Iberian basin-scale circulation and the Portugal boundary current system: A chemical study. *Deep Sea Research, Part I*, *48*(6), 1519–1533. https://doi.org/10.1016/S0967-0637(00)00101-1

Pérez-Folgado, M., Sierro, F. J., Flores, J. A., Cacho, I., Grimalt, J. O., Zahn, R., & Shackleton, N. (2002). Western Mediterranean planktonic foraminifera events and millennial climatic variability during the last 70 kyr. *Marine Micropaleontology*, *48*, 49–70.

Petersen, S. V., Schrag, D. P., & Clark, P. U. (2013). A new mechanism for Dansgaard-Oeschger cycles. *Paleoceanography*, *28*, 24–30. https://doi.org/10.1029/2012PA002364

Peyron, O., Begeot, C., Brewer, S., Heiri, O., Magny, M., Millet, L., et al. (2005). Late-Glacial climatic changes in Eastern France (Lake Lautrey) from pollen, lake-levels, and chironomids. *Quaternary Research*, *64*(2), 197–211. https://doi.org/10.1016/j.yqres.2005.01.006

Peyron, O., Guiot, J., Cheddadi, R., Tarasov, P., Reille, M., de Beaulieu, J.-L., et al. (1998). Climatic reconstruction in Europe for 18,000 yr B.P. from Pollen Data. *Quaternary Research*, *49*(2), 183–196. https://doi.org/10.1006/qres.1997.1961

Pflaumann, U., Sarnthein, M., Chapman, M. R., de Abreu, L., Funnell, B. M., Hüls, M., et al. (2003). Glacial North Atlantic: Sea-surface conditions reconstructed by GLAMAP 2000. *Paleoceanography*, *18*(3), 1065. https://doi.org/10.1029/2002PA000774.

Rahmstorf, S. (2002). Ocean circulation and climate during the past 120,000 years. *Nature*, *419*(6903), 207–214. https://doi.org/10.1038/nature01090

Rasmussen, S. O., Bigler, M., Blockley, S. P., Blunier, T., Buchard, S. L., Clausen, H. B., et al. (2014). A stratigraphic framework for abrupt climatic changes during the last glacial period based on three synchronized Greenland ice-core records: refining and extending the INTIMATE event stratigraphy. *Quaternary Science Reviews*, *106*, 14–28. https://doi.org/10.1016/j.quascirev.2014.09.007

Relvas, P., Barton, E. D., Dubert, J., Oliveira, P. B., Peliz, Á., da Silva, J. C. B., & Santos, A. M. P. (2007). Physical oceanography of the western Iberia ecosystem: Latest views and challenges. *Progress in Oceanography*, *74*(2-3), 149–173. https://doi.org/10.1016/j.pocean.2007.04.021

Renssen, H., & Isarin, R. F. B. (2001). The two major warming phases of the last deglaciation at ~14.7 and ~11.5 ka cal BP in Europe: Climate reconstructions and AGCM experiments. *Global and Planetary Change*, *30*(1-2), 117–153. https://doi.org/10.1016/S0921-8181(01)00082-0

Ribeiro, S., & Amorim, A. (2008). Environmental drivers of temporal succession in recent dinoflagellate cyst assemblages from a coastal site in the North-East Atlantic (Lisbon Bay, Portugal). *Marine Micropaleontology*, *68*(1-2), 156–178. https://doi.org/10.1016/j.marmicro.2008.01.013

Ribeiro, S., Amorim, A., Abrantes, F., & Ellegaard, M. (2016). Environmental change in the Western Iberia Upwelling Ecosystem since the preindustrial period revealed by dinoflagellate cyst records. *The Holocene*, 1–16. https://doi.org/10.1177/0959683615622548

Ridley, H. E., Asmerom, Y., Baldini, J. U. L., Breiten-Bach, S. F. M., Aquino, V. V., Prufer, K. M., et al. (2015). Aerosol forcing of the position of the intertropical convergence zone since ad 1550. *Nature Geoscience*, *8*(3), 195–200. https://doi.org/10.1038/ngeo2353

Risebrobakken, B., Jansen, E., Andersson, C., Mjelde, E., & Hevrøy, K. (2003). A high-resolution study of Holocene paleoclimatic and paleoceanographic changes in the Nordic Seas. *Paleoceanography*, *18*(1), 1017. https://doi.org/10.1029/2002PA000764

Rochon, A., de Vernal, A., Turon, J. L., Matthiessen, J., & Head, M. J. (1999). Distribution of recent dinoflagellate cysts in surface sediments from the North Atlantic Ocean and adjacent seas in relation to sea-surface parameters. *American Association of Stratigraphic Palynologists Contributions Series*, *35*, 1–146.

Ruddiman, W. F. (2003). Orbital insolation, ice volume, and green- house gases. *Quaternary Science Reviews*, *22*(15-17), 1597–1629. https://doi.org/10.1016/S0277-3791(03)00087-8

Salgueiro, E., Naughton, F., Voelker, A. H. L., de Abreu, L., Alberto, A., Rossignol, L., et al. (2014). Past circulation along the western Iberian margin: a time slice vision from the last glacial to the Holocene. *Quaternary Science Reviews*, *106*, 316–329. https://doi.org/10.1016/j.quascirev.2014.09.001

Salgueiro, E., Voelker, A. H. L., de Abreu, L., Abrantes, F., Meggers, H., & Wefer, G. (2010). Temperature and productivity changes off the western Iberian margin during the last 150 ky. *Quaternary Science Reviews*, *29*, 680–695. https://doi.org/10.1016/j.quascirev.2009.11.013

Sanchez Goñi, M. F., Landais, A., Fletcher, W. J., Naughton, F., Desprat, S., & Duprat, J. (2008). Contrasting impacts of Dansgaard–Oeschger events over a western European latitudinal transect modulated by orbital parameters. *Quaternary Science Reviews*, *27*(11-12), 1136–1151. https://doi.org/10.1016/j.quascirev.2008.03.003

Sánchez, R. F., & Relvas, P. (2003). Spring–summer climatological circulation in the upper layer in the region of Cape St. Vincent, Southwest Portugal. *ICES Journal of Marine Science*, *60*(6), 1232–1250. https://doi.org/10.1016/S1054-3139(03)00137-1

Sánchez, R. F., Relvas, P., Martinho, A., & Miller, P. (2008). Physical description of an upwelling filament west of Cape St. Vincent in late October 2004. *Journal of Geophysical Research*, *113*, C07044. https://doi.org/10.1029/2007JC004430

Santer, B. D., Po-Chedley, S., Zelinka, M. D., Cvijanovic, I., Bonfils, C., Durack, P. J., et al. (2018). Human influence on the seasonal cycle of tropospheric temperature. *Science*, *361*, 245.

Sarnthein, M., Pflaumann, U., & Weinelt, M. (2003). Past extent of sea ice in the northern North Atlantic inferred from foraminiferal paleotemperature estimates. *Paleoceanography*, *18*(2), 1047. https://doi.org/10.1029/2002PA000771

Schiebel, R., & Hemleben, C. (2005). Modern planktic foraminifera. *Paläontologische Zeitschrift*, *79*(1), 135–148. https://doi.org/10.1007/BF03021758

Schneider, B., Leduc, G., & Park, W. (2010). Disentangling seasonal signals in Holocene climate trends by satellite-model-proxy integration. *Paleoceanography*, *25*, PA4217. https://doi.org/10.1029/2009PA001893

Seager, R., & Battisti, D. S. (2007). Challenges to our understanding of the general circulation: Abrupt climate change. In T. Schneider & A. H. Sobel (Eds.), *Global circulation of the atmosphere*. Princeton, N.J.: Princeton University Press.

Severinghaus, J., Sowers, T., Brook, E., Alley, R. B., & Bender, M. L. (1998). Timing of abrupt climate change at the end of the Younger Dryas interval from thermally fractionated gases in polar ice. *Nature*, *391*, 141–146. https://doi.org/10.1038/34346

Skinner, L. C., & Shackleton, N. J. (2004). Rapid transient changes in northeast Atlantic deep water ventilation age across termination I. *Paleoceanography*, *19*, PA2005. https://doi.org/10.1029/2003PA000983

Sousa, F. M., & Bricaud, A. (1992). Satellite-derived phytoplankton pigment structures in the Portuguese upwelling area. *Journal of Geophysical Research*, *97*(C7), 11343–11356. https://doi.org/10.1029/92JC00786

Sun, D., Gagan, M. K., Cheng, H., Scott-Gagan, H., Dykoski, C. A., Edwards, R. L., & Su, R. (2005). Seasonal and interannual variability of the Mid-Holocene East Asian monsoon in coral δ18O records from the South China Sea. *Earth and Planetary Science Letters*, *237*(1-2), 69–84. https://doi.org/10.1016/j.epsl.2005.06.022

Tabone, I., Blasco, J., Robinson, A., Alvarez-Solas, J., & Montoya, M. (2018). The sensitivity of the Greenland ice sheet to glacial-interglacial oceanic forcing. *Climate of the Past*, *14*, 455–472. https://doi.org/10.5194/cp-14-455-2018

Teles-Machado, A., Peliz, Á., McWilliams, J. C., Cardoso, R. M., Soares, P. M. M., & Miranda, P. M. A. (2015). On the year-to-year changes of the Iberian Poleward Current. *Journal of Geophysical Research: Oceans*, *120*, 4980–4999. https://doi.org/10.1002/2015JC010758

Teles-Machado, A., Peliz, Á., McWilliams, J. C., Couvelard, X., & Ambar, I. (2015). Circulation on the Northwestern Iberian Margin: Vertical structure and seasonality of the alongshore flows. *Progress in Oceanography*, *140*, 134–153. https://doi.org/10.1016/j.pocean.2015.05.021

Tierney, J. E., & Tingley, M. P. (2018). BAYSPLINE: A new calibration for the alkenone paleothermometer. *Paleoceanography and Paleoclimatology*, *33*, 281–301. https://doi.org/10.1002/2017PA003201

van Helmond, N. A. G. M., Hennekam, R., Donders, T. H., Bunnik, F. P. M., de Lange, G. J., Brinkhuis, H., & Sangiorgi, F. (2015). Marine productivity leads organic matter preservation in sapropel S1: Palynological evidence from a core east of the Nile River outflow. *Quaternary Science Reviews*, *108*, 130–138. https://doi.org/10.1016/j.quascirev.2014.11.014

Van Meerbeeck, C. J., Renssen, H., Roche, D. M., Wohlfarth, B., Bohnck, S. J. P., Bos, J. A. A., et al. (2011). The nature of MIS 3 stadial-interstadial transitions in Europe: New insights from model-data comparisons. *Quaternary Science Reviews*, *30*(25-26), 3618–3637. https://doi.org/10.1016/j.quascirev.2011.08.002

van Nieuwenhove, N., Baumann, A., Mathiessen, J., Bonnet, S., & de Vernal, A. (2016). Sea surface conditions in the southern Nordic Seas during the Holocene based on dinoflagellate cyst assemblages. *The Holocene*, *26*(5), 722–735. https://doi.org/10.1177/0959683615618258

Voelker, A. H. L., & de Abreu, L. (2011). In H. Rashid, L. Polyak, & E. Mosley-Thompson (Eds.), *A review of abrupt climate change events in the Northeastern Atlantic Ocean (Iberian Margin): Latitudinal, longitudinal, and vertical gradients. abrupt climate change: mechanisms, patterns, and impacts*. Washington, D.C: American Geophysical Union. https://doi.org/10.1029/2010GM001021

Vogelsang, E., Sarnthein, M., Pflaumann, U., (2001). d18O Stratigraphy, chronology, and sea surface temperatures of Atlantic sediment records (GLAMAP-2000 Kiel). Reports, Institut für Geowissenschaften 13.

Waelbroeck, C., Labeyrie, L., Duplessy, J. C., Guiot, J., Labracherie, M., Leclaire, H., & Duprat, J. (1998). Improving past sea surface temperature estimates based on planktonic fossil faunas. *Paleoceanography*, *13*, 272–283.

Wary, M., Eynaud, F., Kissel, C., Londeix, L., Rossignol, L., Lapuyade, L., et al. (2018). Spatio-temporal dynamics of hydrographic reorganizations and iceberg discharges at the junction between the Northeast Atlantic and Norwegian Sea basins surrounding Heinrich event 4. *Earth and Planetary Science Letters*, *481*, 236–245. https://doi.org/10.1016/j.epsl.2017.10.042

Wary, M., Eynaud, F., Rossignol, L., Lapuyade, J., Gasparotto, M.-C., Londeix, L., et al. (2016). Norwegian Sea warm pulses during Dansgaard-Oeschger stadials: Zooming in on these anomalies over the 35-41 ka cal BP interval and their impacts on proximal European ice-sheet dynamics. *Quaternary Science Reviews*, *151*, 255–272. https://doi.org/10.1016/j.quascirev.2016.09.011

Wary, M., Eynaud, F., Rossignol, L., Zaragosi, S., Sabine, M., Castéra, M.-H., & Billy, I. (2017). The southern Norwegian Sea during the last 45 ka: Hydrographical reorganizations under changing ice-sheet dynamics. *Journal of Quaternary Science*, *32*(7), 908–922. https://doi.org/10.1002/jqs.2965

Wary, M., Eynaud, F., Sabine, M., Zaragosi, S., Rossignol, L., Malaizé, B., et al. (2015). Stratification of surface waters during the last glacial millennial climatic events: A key factor in subsurface and deep-water mass dynamics. *Climate of the Past*, *11*(11), 1507–1525. https://doi.org/10.5194/cp-11-1507-2015

Williams, G. L., Fensome, R. A., & MacRae, R. A. (2017). *The Lentin and Williams Index of fossil dinoflagellates*, *American Association of Stratigraphic Palynologists Contributions Series*, (2017th ed., Vol. 48, p. 1097).

Wu, H., Guiot, J., Brewer, S., & Guo, Z. (2007). Climatic changes in Eurasia and Africa at the last glacial maximum and mid-Holocene: reconstruction from pollen data using inverse vegetation modelling. *Climate Dynamics*, *29*(2-3), 211–229. https://doi.org/10.1007/s00382-007-0231-3

Wunsch, C. (2006). Abrupt climate change: An alternative view. *Quaternary Research*, *65*(02), 191–203. https://doi.org/10.1016/j.yqres.2005.10.006

Zonneveld, K. A. F., Marret, F., Versteegh, G. J. M., Bogus, K., Bonnet, S., Bouimetarhan, I., et al. (2013). Atlas of modern dinoflagellate cyst distribution based on 2405 data points. *Review of Palaeobotany and Palynology*, *191*, 1–197. https://doi.org/10.1594/PANGAEA.818280

Zonneveld, K. A. F., & Pospelova, V. (2015). A determination key for modern dinoflagellate cysts. *Palynology*, *39*(3), 387–409. https://doi.org/10.1080/01916122.2014.990115, https://www.marum.de/en/Modern_Dinocyst_Key.html

Zonneveld, K. A. F., Versteegh, G. J. M., & Kodrans-Nsiah, M. (2008). Preservation and organic chemistry of Late Cenozoic organic-walled dinoflagellate cysts: a review. *Marine Micropaleontology*, *68*(1-2), 179–197. https://doi.org/10.1016/j.marmicro.2008.01.015